ARL-TR-9352 ● Nov 2021

DEVCOM ARMY RESEARCH LABORATORY

Headform Kinematic Comparison Across Three Blunt Impact Testing Modes

by Mark Jesunathadas, Trenton E Gould, Thomas A Plaisted, Ryan J Neice, Elizabeth D Edwards, Tiffany Landry, Michael Kleinberger, and Scott G Piland

NOTICES

Disclaimers

The findings in this report are not to be construed as an official Department of the Army position unless so designated by other authorized documents.

Citation of manufacturer's or trade names does not constitute an official endorsement or approval of the use thereof.

Destroy this report when it is no longer needed. Do not return it to the originator.

ARL-TR-9352 ● Nov 2021

Headform Kinematic Comparison Across Three Blunt Impact Testing Modes

Mark Jesunathadas, Trenton E Gould, Elizabeth D Edwards, Tiffany Landry, and Scott G Piland
The University of Southern Mississippi

Thomas A Plaisted and Michael Kleinberger
Weapons and Materials Research Directorate,
DEVCOM Army Research Laboratory

Ryan J Neice
Oak Ridge Associated Universities

REPORT DOCUMENTATION PAGE

Form Approved
OMB No. 0704-0188

1. REPORT DATE *(DD-MM-YYYY)*	2. REPORT TYPE	3. DATES COVERED (From - To)
November 2021	Technical Report	1 May 2019–31 August 2021

4. TITLE AND SUBTITLE
Headform Kinematic Comparison Across Three Blunt Impact Testing Modes

5a. CONTRACT NUMBER

5b. GRANT NUMBER

5c. PROGRAM ELEMENT NUMBER

6. AUTHOR(S)
Mark Jesunathadas, Trenton E Gould, Thomas A Plaisted, Ryan J Neice, Elizabeth D Edwards, Tiffany Landry, Michael Kleinberger, and Scott G Piland

5d. PROJECT NUMBER

5e. TASK NUMBER

5f. WORK UNIT NUMBER

7. PERFORMING ORGANIZATION NAME(S) AND ADDRESS(ES)
DEVCOM Army Research Laboratory
ATTN: FCDD-RLW-MA
Aberdeen Proving Ground, MD 21005

8. PERFORMING ORGANIZATION REPORT NUMBER
ARL-TR-9352

9. SPONSORING/MONITORING AGENCY NAME(S) AND ADDRESS(ES)

10. SPONSOR/MONITOR'S ACRONYM(S)

11. SPONSOR/MONITOR'S REPORT NUMBER(S)

12. DISTRIBUTION/AVAILABILITY STATEMENT
Approved for public release: distribution unlimited.

13. SUPPLEMENTARY NOTES
ORCID IDs: Thomas A Plaisted 0000-00032903-3263; Ryan J Neice 000-0002-0550-0907

14. ABSTRACT

This report delineates and standardizes methods to impact an anthropomorphic test device (ATD) donning an Advanced Combat Helmet (ACH) across three impact test machine configurations common to sport (monorail, basket drop, and pneumatic ram), and evaluates the linear and angular kinematic response during blunt impacts. Prior to impact testing at matched velocities, we developed drop tests to determine whether drop mass should be accounted for between configurations. Impact testing of a male 50% Hybrid III head with a 6 degree-of-freedom angular rate sensor package donning an ACH was completed at seven prescribed locations at impact velocities of 10, 14, and 17 ft/s (ram) and 10 and 14 ft/s (drop). Dependent variables included peak resultant linear acceleration (PLA), peak resultant angular acceleration (PAA), and peak resultant angular velocity of the ATD headform center of mass. Finite element (FE) simulations of the ram tests were conducted post-hoc. Differences in drop mass alone did not result in meaningful differences in PLA, but adjusting impact velocity to account for mass differences did. In contrast, matching drop impact velocity produced the most similar PLAs between ATDs of different masses. Across configurations, the ram produced the lowest PLAs and PAAs, whereas the monorail typically resulted in the greatest PAA values. These results are partially explained by a set of simplified equations and confirmed through FE simulations.

15. SUBJECT TERMS
combat helmet, blunt impact, test and evaluation, headform, linear and angular kinematics

16. SECURITY CLASSIFICATION OF:			17. LIMITATION OF ABSTRACT	18. NUMBER OF PAGES	19a. NAME OF RESPONSIBLE PERSON
a. REPORT	b. ABSTRACT	c. THIS PAGE			Thomas A Plaisted
Unclassified	Unclassified	Unclassified	UU	43	19b. TELEPHONE NUMBER (Include area code) (410) 306-4960

Contents

List of Figures

List of Tables

1. Introduction

Soldiers in combat and in training face varied environments that pose the threat of injury, including head injury. Both ballistic and blunt head impact threats require the use of personal protective equipment, namely, a combat helmet. Currently, protection performance is assessed on the ability of the helmet to minimize head linear kinematics, which can result in brain injury. The Advanced Combat Helmet (ACH), for example, is evaluated on its ability to mitigate blunt impact forces that result in head translational motion, measured currently by uniaxial linear acceleration.[1,2] However, it has become well established that rapid rotation of the head can induce strain and shearing of brain tissue that can result in brain injury.[3–6] To fully characterize the ability of combat helmets to mitigate brain injury from blunt impacts, these helmets should also be assessed on the ability to minimize head angular kinematics. The US Army blunt impact standard (AR/PD 10-02)[1] utilizes a monorail-style drop test, in which angular motion of an anthropomorphic test device (ATD) head is constrained.[1,2,7,8] Thus, the current Army standard for the ACH does not address the threat of angular head kinematics to the Soldier. Thus, the US Army may need to consider additional rotational requirements to provide a comprehensive evaluation of the protective capabilities of the ACH.

In sport, there are varying methods for assessing a helmet's ability to protect the head from excessive rotation.[9–12] For example, American football helmets, which are certified by the National Operating Committee on Standards and Equipment (NOCSAE), adopted the use of a pneumatic ram to impact a NOCSAE ATD, which is mounted on a male 50% Hybrid III neck attached to a sliding table.[9] In contrast, bicycle helmet researchers, manufacturers, and performance rating systems utilize a method in which an ATD head rests on a ring (alternately referred to as a basket) without a neck or mount attachment and is dropped onto an angled anvil.[10–12] Notably, these two approaches model different impact events, wherein drop tests model fall related impacts against an immovable object, while ram-type tests model the collisions of two bodies of comparable mass that are each free to rebound after impact. Therefore, the purpose of this technical report is twofold: 1) delineate and standardize methods used to impact an ATD donning an ACH across three different impact test machine configurations (monorail, basket, and pneumatic ram) common to sport and 2) evaluate the linear and angular kinematic response of an ATD donning an ACH during blunt impacts across these three machine configurations.

1.1 Military Relevance

US Army Soldiers' operational and training environments pose a variety of injurious threats to the head and brain of Warfighters. Easily recognizable blunt

impact threats to the head of the modern Warfighter include motor vehicle accidents, falling while maneuvering by foot, associated secondary impacts from blast wave exposure, and exposure during paratrooper operations.[13,14] These threats are underscored by the incidence of 16,198 diagnosed traumatic brain injuries (TBIs) among military service members in 2020, the majority of which were classified as a concussion or mild TBI.[15] More specifically, a study of Soldiers at Fort Bragg, North Carolina, between 1999 and 2000 found that approximately 23% of surveyed Soldiers (2,337) sustained a TBI after joining the Army and more than twice as many paratroopers than non-paratroopers reported sustaining a TBI after joining the Army.[14]

Even in mild cases of brain injury associated with blunt impacts, both short- and long-term impairments can occur including dizziness, memory loss, difficulty concentrating, visual impairment, headaches, and irritation. Such impairments can compromise the survivability and safety of the Soldier and the unit, mission success, and Soldier lethality. Additionally, the long-term consequences can be detrimental to the health of the Soldier, degrading readiness, and can have a significant cost to the United States over the life of the Soldier. Thus, the need to appropriately ascertain and manage both the linear and angular kinematic threats to Soldiers' heads is of critical importance.

2. Methods

ATC-MMTB-029, Rev E, describes the specific ATD pose (i.e., position and orientation) and blunt impact locations used to evaluate the ability of an ACH to mitigate linear head kinematics during a guided monorail drop.[2] Our foundational framework to developing methods that evaluate linear and angular acceleration was to approximate these ATD poses and impact locations using surrogate test methods. Specifically, we attempted to the match the pose and impact location specified by the Aberdeen Test Center's (ATC's) blunt impact testing procedure. To this end, we utilized three separate impact test machine configurations often used for evaluating sport helmets: 1) pneumatic ram, 2) guided monorail drop, and 3) guided basket drop. We constrained all test machine configurations to utilize the impactor head specified by NOCSAE Doc ND081-18am19a[9] to make comparisons across machine configurations.

Because the neck has an influence on the angular kinematics of the head, the first two methods included a male 50% Hybrid III head connected to a surrogate flexible neck (male 50% Hybrid III). In contrast, the basket drop method does not connect the headform to the test apparatus, thereby allowing the headform to rotate upon impact without constraint. Custom mounts were fabricated to affix the ATD to each

impact machine configuration. Helmet fit was standardized based on the Operator's Manual for ACH.[1] Test velocities included 10, 14, and 17 ft/s. Additional velocities were also used to match the energy or momentum between drop methods (see the Drop Mass sections).

2.1 Pneumatic Ram

The pneumatic ram used a pneumatically driven rod affixed with an impactor head to impact the ATD. This format is currently used by the National Football League and NOCSAE in the evaluation of protective headgear in football.[16,17] The system operated such that just prior to impact the rod was in guided free flight. The ATD head and neck were mounted to a sliding table that was free to move in the direction of impact. An example of the front impact location and corresponding ATD pose is shown in Fig. 1. Additional poses can be seen in supplementary material (Figs. A-1 to A-4 in the Appendix).

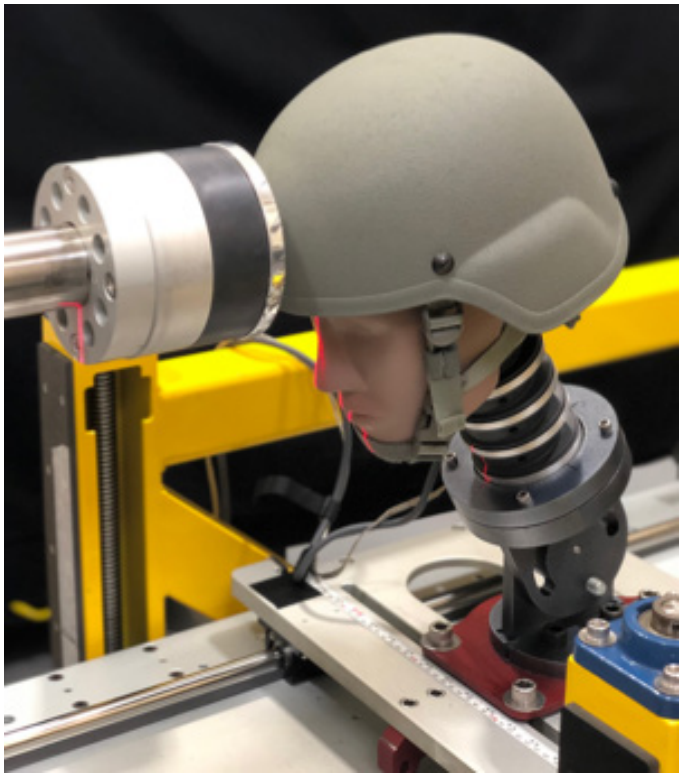

Fig. 1 Pneumatic ram machine configuration with male 50% Hybrid III head and neck ATD in pose for the front impact location

2.2 Guided Monorail

The guided monorail dropped the ATD onto the anvil at a prescribed test velocity. This format most closely resembles the Army's helmet evaluation format with the

exception that a male 50% Hybrid III neck is used to attach the ATD head (Hybrid III or NOCSAE) to the monorail, thus enabling angular motion of the ATD. An example of the front impact location and corresponding ATD pose is shown in Fig. 2. Additional poses can be seen in supplementary material (Figs. A-5 to A-8 in the Appendix).

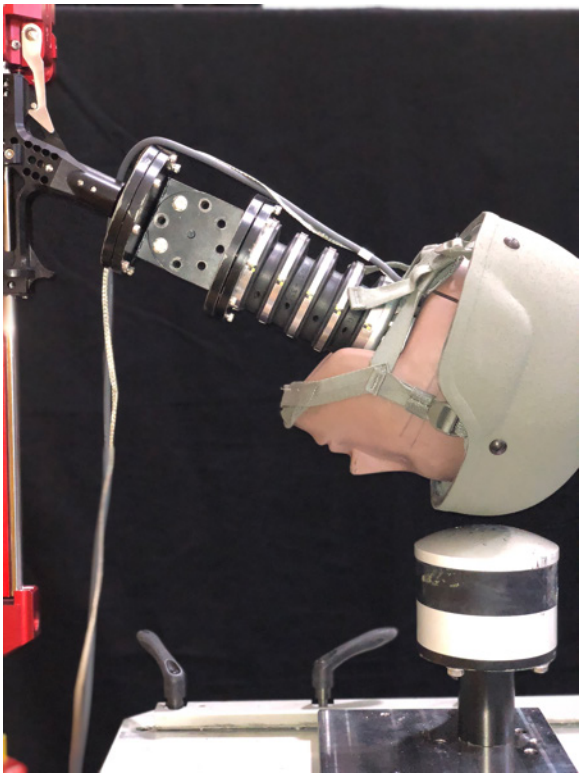

Fig. 2 Guided monorail machine configuration with male 50% Hybrid III head and neck ATD pose for the front impact location

2.3 Basket Drop

The basket drop uses the monorail drop rig to drop a headform by means of a semi-circular ring (basket) onto the anvil. The headform is unconstrained during impact and is only tethered to the machine by means of a rope attached to the base of the headform. This impact format has been adopted to evaluate bicycle and motorcycle helmets.[10,18] To position the ATD, a flat surface was placed on the base of the headform to provide a surface for a digital inclinometer to measure the orientation of the ATD with respect to the basket. An example of the front impact location and corresponding ATD pose is shown in Fig. 3. Additional poses can be seen in supplementary material (Figs. A-9 to A-12 in the Appendix).

Fig. 3 Basket drop male 50% Hybrid III ATD pose for the front impact location

2.4 Standardized Description of Impact Pose

A relatively simple and reliable approach to describe the pose of a body is by means of describing the current position of a point P (P_2) on the body in relation to a previous position of point P (P_1). This can be done by attaching a local or fixed frame to the body and describing the geometric relation between the coordinate frames associated with P_1 and P_2. The geometric relations between the coordinate frames can be described in terms of rotations and translations about and along the x, y, and z axes of the predefined coordinate system. However, the order of rotations as well as whether the rotations are about a local or fixed coordinate frame must be considered. Figure 4 highlights how the order of rotations can drastically affect the pose of a rigid body in space.

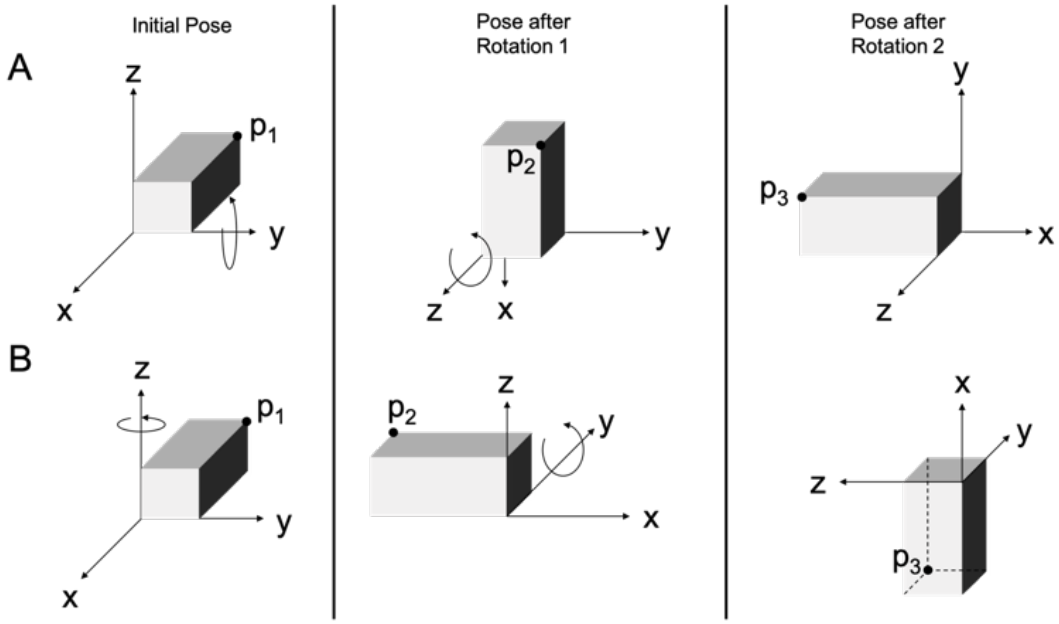

Fig. 4 A) 90° rotations about the local y-axis and then local z-axis and B) 90° rotations about the local z-axis and then local y-axis. The order of rotation proceeds from left to right.

In Fig. 5, we detail the method used to describe ATD impact pose, which will help to standardize impact location on the ATD by leveraging the order or rotation phenomena described earlier. However, unlike the example in Fig. 4, the mounts used for ATD impact testing often comprise multi-linked joints that serve to translate and rotate the ATD. Figure 5 shows the pneumatic ram setup diagramed as a multi-link mount. Note the principles used to describe the pneumatic ram mount can be extended to many other mounts used in head impact testing.

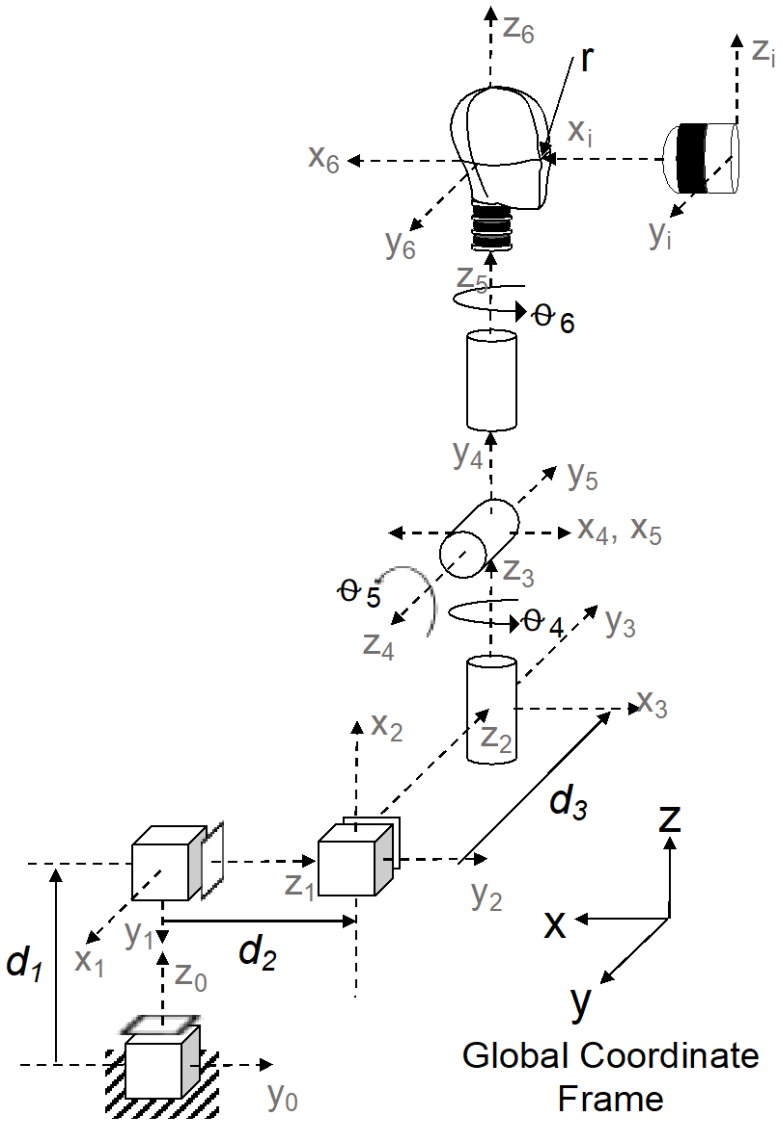

Fig. 5 Diagram of a multi-link mount with coordinate frames for each link established according to the Denavit–Hartenberg (DH) Convention. The mount is oriented in a reference position with the impactor aligned to a reference point r on the ATD.

The method requires the following steps:

1) Identify the model of the ATD and impactor/anvil. If the design and dimensions of the ATD or impactor/anvil are novel, these should be provided.

2) Define a global coordinate system in a fashion that can be used to aid in the description of a reference mount pose.

3) Establish a reference mount pose. We propose that this reference pose result in a prominent, defined, and accessible feature of the ATD (point r) to be coincident with the center of the impactor/anvil.

4) Define the coordinate frames for each link of the mount's joints in the reference pose. A universal method of defining these coordinate frames is through the use of the DH Convention (see Denavit and Hartenberg[19] and Spong et al.[20]) for a detailed description of the DH Convention).

   Briefly, the DH Convention defines coordinate frames for each link as follows: a) the z_i-axis of each coordinate frame (frames 0 – n) is aligned with the axis of actuation for joint i + 1 (e.g., z_0 is the axis of actuation for joint 1); b) the x-axis of the coordinate frame i intersects the z-axis of coordinate frame i-1; c) the x-axis of the coordinate frame i is perpendicular to the z-axis of coordinate frame i-1; d) the y-axis for each coordinate frame is then defined according to the right-hand rule; and e) when possible, we suggest aligning the origin of each coordinate frame at the corresponding joint center for convenience, but this is not a necessary requirement and other locations for a coordinate frame's origin may prove more convenient for some mounts. Note the x- and y-directions of the base coordinate frame (frame 0) are arbitrary as long as the coordinate frame is right-handed. Once the 0-coordinate frame is established, each coordinate frame i is established using coordinate frame i-1.

5) Establish the reference pose, define the pose of each link i with respect to the previous link (i-1). To establish the pose for each impact location (e.g., front boss), specify the variable DH parameters for each link with respect to the reference pose. Note the parameters that are constant and variable (at minimum a, α and θ are constant for prismatic joints, while a, α and d are constant for revolute joints). Using the DH Convention reduces the required parameters to fully define the pose of each link from six to four. The four DH parameters (a, α, d, and θ) are defined in Table 1.

Table 1 Definition of the four DH parameters

DH parameter	Definition
a_i, "link length"	Distance between axes z_{i-1} and z_i, measured along axis x_i
α_I, "link twist"	Angle from z_{i-1} to z_i about the x_i-axis measured according to the right-hand rule
d_i, "link offset"	Distance from the origin of coordinate frame i-1 to the intersection of axis x_i and z_{i-1} measured along z_{i-1}-axis
θ_I, "joint angle"	Angle from x_{i-1} to x_i about the z_{i-1}-axis measured according to the right-hand rule

6) Identify the pose of the impactor/anvil for the reference pose and each impact location in the following manner at the point of impact: a) assign a coordinate frame to the impactor/anvil, such that the origin is located at the impact surface's center, one axis is perpendicular to the impact surface, and the other two axes follow the right hand-rule; b) assign a coordinate frame for the ATD such that the origin is at the reference point (point r), but the axes directions are defined as they were in step 4 (note this step can be skipped if the impactor/anvil coordinate frame is going to be described in relation to the global coordinate system); and c) describe the series of translations and rotations that would result in identical coordinate poses of the ATD coordinate frame in its reference pose or the global coordinate system with the impactor coordinate system, noting that the order of rotations matter (see Fig. 4). Note that for many test setups, the impactor/anvil coordinate systems and the ATD or global coordinate system will align without the need for any coordinate frame rotations and this pose will be fixed throughout testing. We emphasize that the pose should be described at the moment of impact.

7) In a manner similar to step 6, provide the velocity vector of the moving system in relation to the fixed system. The goal is to describe the rotations that align the velocity vector with one of the coordinate axes of the stationary system. In many testing arrangements, the velocity vector will initially be aligned with one of the axes defined for the ATD or impactor/anvil for the reference pose (see steps 3–5). For further details on DH parameters used in impact testing, see Jesunathadas et al.[21]

8) The DH parameters and mount design for the ATD on the pneumatic ram method, which result in the same impact locations as that prescribed by ATC Internal Operating Procedure (IOP),[2] are shown in Fig. 5 and Table 2.

Table 2 DH parameters and mount adjustment parameters the seven impact locations used for the ACH on the pneumatic ram

Mount DH parameters					Adjustment parameters					
Links	a_i (mm)	α_i (°)	d_i (mm)	θ_i (°)	Pose	d_1 (mm)	d_3 (mm)	θ_4 (°)	θ_5 (°)	θ_6 (°)
1	0	–90	d_{1r}[a]	0	Crown[b]	287	0	0	–85	0
2	0	90	d_{2r} = kiss	–90	Front[#]	3	0	0	–26	0
3	0	90	d_{3r}[a]	90	Rear[b]	14	0	0	–20	180
4	0	90	95	q_{4r}[a] = 0	L. Side[b]	–24	0	0	–20	–90
5	0	–90	0	q_{5r}[a] = 0	R. Side[b]	–24	0	0	–20	90
6	0	0	310	q_{6r}[a] = 180	L. Nape[c]	–7	0	0	0	–150
					R. Nape[c]	–7	0	0	0	150

[a] Joint variables d_1, d_3, θ_4, θ_5, and θ_6 were set so that the line passing through the center of the impactor (x_i) passed through the point r, made by the intersection of the midsagittal and transverse (basic) plane with the ATD neck vertical (i.e., z_6 is parallel to the global z-axis). Joint value d_2 is adjusted so that the impact point on the ATD head is at a horizontal distance of no more than 1 inch from the impactor rod's face as the rod just begins guided free flight (kiss). All other joint values are constant and a function of the mount design. Mount DH nominal values ± 10 mm and ± 0.5°.

Adjustment parameters are nominal but vary across helmets:

[b] d_1 and d_2 values adjusted to impact the apex of the helmet; # d_1 adjusted to impact 0.5 inch above the night vision goggle hole.

[c] d_1 and d_2 adjusted so impactor impacts helmet as close to but without impacting nape bolts. Adjustment q parameters are nominal ± 0.3°.

2.5 Accounting for Drop Masses

The work-energy equations indicate that mass should not influence the peak resultant linear acceleration (PLA) of a free-falling rigid body during an impact event (Eq. 1). Rather the equation predicts that PLA is a function of impact velocity (v_i) or drop height (h), gravity (g), and the maximum compression distance of the impact surface (Δx):

$$a_p = \frac{v_i^2}{\Delta x} = \frac{2g(h+\Delta x)}{\Delta x} \quad (1)$$

However, a typical drop impact test of an ATD may not meet all the assumptions of these equations and may involve more complicated material characteristics and boundary conditions. In such drop impacts, it is unclear if the drop mass influences the PLA values of the ATD. Thus, drop tests that evaluate the impact performance (measured by peak acceleration) of a helmet across ATDs with similar geometries but different masses (e.g., with and without an attached ATD neck) may need to account for mass differences. Practical ways to account for mass differences across ATD setups are to match the kinetic energy or momentum of the dropped system just prior to impact to a reference impact. Therefore, we matched the kinetic energy and momentum to a reference impact in two different scenarios. In the first scenario, the ATD geometry was the same (Department of Transportation [DOT]-C headform) and ATD mass varied. We then adjusted drop height to match the kinetic energy or momentum of the reference impact. Impacts were also conducted

in which drop height was not adjusted and impact velocity was matched between the ATD setups of differing masses. In the second scenario, ATD geometry differed along with ATD mass in that an ATD neck (male 50% Hybrid III) was either attached or not attached to a male 50% Hybrid III ATD head. Drop heights for each setup were adjusted to match the kinetic energy or momentum of a reference impact of the opposing setup. Additional details for each scenario are provided in the following sections.

2.5.1 Same ATD Geometry: DOT-C

Impacts to the crown of the DOT-C headform were performed using a guided monorail drop tower. The DOT-C headform pose was such that its base was parallel to the ground, the anterior portion faced the drop rail, and the midsagittal plane aligned with the drop rail. The mass of the DOT-C headform was manipulated by attaching couplers to the headform of two different masses (4.93 or 5.69 kg). The DOT-C headform was dropped onto a 2.54-cm Modular Elastic Programmer (MEP with Shore A 60). The 4.93-kg system was dropped from a height of 30 cm. To evaluate the influence of mass on the impact acceleration of the headform, the 5.69-kg system was dropped from heights that matched the impact kinetic energy (E_K), momentum (p), and velocity (v_i) of the 4.93-kg system (Table 3).

Table 3 DOT-C drop conditions and parameters

Condition	d (cm)	KE (J)	p (kg·m/s)
Reference	30.0	14.08	11.78
E_k match	26.0	13.85	12.56
p match	21.8	11.63	11.51
v_i match	30.0	16.10	13.54

Note: Values of the same color indicate matched parameters.

2.5.2 Different ATD Geometry: Male 50% Hybrid III

The male 50% Hybrid III ATD donning an ACH was dropped using the guided monorail (unhelmeted drop mass: 10.9 kg) and basket drop (unhelmeted drop mass: 4.8 kg) methods. The addition of the neck in the guided monorail drop served to increase the mass and alter the geometry of the ATD. The ATD drop height was adjusted so that ATD was dropped at an equivalent energy (72.3 J) and an equivalent velocity (10 ft/s) between methods for all seven impact locations.

2.6 Finite Element Simulations

A US Army Combat Capabilities Development Command Army Research Laboratory–developed finite element analysis (FEA) model of the pneumatic ram was used. The FEA model has been validated against experimental impacts using Correlation and Analysis Software (CORA; Partnership for Dummy Technology and Biomechanics, Gaimersheim, Germany) scoring for both bareheaded and helmeted pneumatic ram impacts at 10, 14, and 17 ft/s at front, rear, sides, napes, and crown impact locations. CORA scoring is commonly used as a correlation rating method, as it considers the phase, slope, and magnitude of a given data trace, as well as a corridor method that scores distance between a scored and targeted trace at any point in time. Averaged across all ACH helmeted simulation, the CORA scores for linear acceleration, angular acceleration, and angular velocity outputs were 0.708, 0.558, and 0.728, respectively.

Finite element modeling was used to further validate our findings and provide limits on the extent mass properties have ATD kinematic response. The FEA model was used to explore the effects and relationship between impactor mass and inertial properties. The FEA model includes the impactor rod, ATD head–neck, ACH helmet, and carriage mass. The impactor, ACH, head and neck, and carriage comprised 24,776, 77,328, 69,908, and 1,364 elements, respectively. The model was adjusted such that the mass of the simulated impactor was increased by four times, from 16.7 kg to 66.8 kg, and impacted an ATD-complex of mass 23.6 kg. Additionally, FEA simulations of front and left side impacts at 14 ft/s, which matched impactor mass to ATD complex mass were run. Each simulation provides linear acceleration, angular acceleration, and angular velocity time-histories for each case.

2.7 Instrumentation

2.7.1 DOT-C

Linear acceleration of the DOT-C headform was acquired with a uniaxial accelerometer (model 353B18, PCB Piezotronic Inc., Depew, New York). High-speed video of the first impact of each location across test machine configurations was obtained using a Phantom V611 camera (1000–3000 fps; Vision Research, Wayne, New Jersey).

2.7.2 Male 50% Hybrid III

Linear acceleration and angular velocity signals of the male 50% Hybrid III were obtained with a DTS 6 degree-of-freedom (6DOF) system (6DX PRO, 2000 g,

18,000°/s, DTS, Seal Beach, California). A second-order low-pass Butterworth filter implemented in MATLAB (MathWorks, Natick, Massachusetts) was used to condition the linear acceleration (corner frequency 300 Hz) and angular velocity signals (corner frequency 258 Hz).[3] Angular velocity signals were then differentiated to obtain angular accelerations. Kinematic variables included PLA and peak resultant angular accelerations (PAA) as well as peak resultant angular velocity (PAV). High-speed video of the first impact of each location across test machine configurations was obtained using a Phantom V611 camera (1000–3000 fps; Vision Research) for the 10-, 14-, and 17-ft/s test velocities.

3. Statistics

For all statistical tests, Bonferroni adjustments were used for multiple comparisons. An alpha level of 0.05 was considered significant. Greenhouse–Geisser corrections were used for violations of sphericity.

3.1 Accounting for Drop Mass: Same ATD Geometry

A one-way repeated measure (drop mass) analysis of variance (ANOVA) was used to compare the PLA values from the energy (E_k), momentum] (p), and velocity matched (v_i) drops to the reference drop.

3.2 Accounting for Drop Mass: Different ATD Geometry

Two separate 2 × 7 (drop mass × impact location) repeated measures (impact location) ANOVA were used to compare PLA values. The first ANOVA compared the PLA values between monorail and basket drop drop masses when the impact energies were matched. The second ANOVA compared the PLA values between the two drop masses when the drop velocities were matched. Simple effects analysis was used to compare PLA between the two drop masses at each impact location.

3.3 Velocity Matched Across Platforms

A 3 × 7 (machine configuration × impact location) repeated measures (impact location) analysis of covariance (ANCOVA) was used to compare PLA, PAA, and PAV values. Simple effects analysis was used to compare outcome measure values between machine configurations at each impact location.

4. Results

4.1 Accounting for Drop Mass: Same ATD Geometry

The peak linear accelerations of the DOT-C headform differed statistically between the reference and other three conditions ($p \leq 0.015$). However, the 95% confidence interval (CI) of the mean difference between the reference and velocity matched condition was 2.4–11.3 g, but was 13.1–26.1 and 33.1–42.5 g for the energy and momentum matched conditions, respectively (Fig. 6).

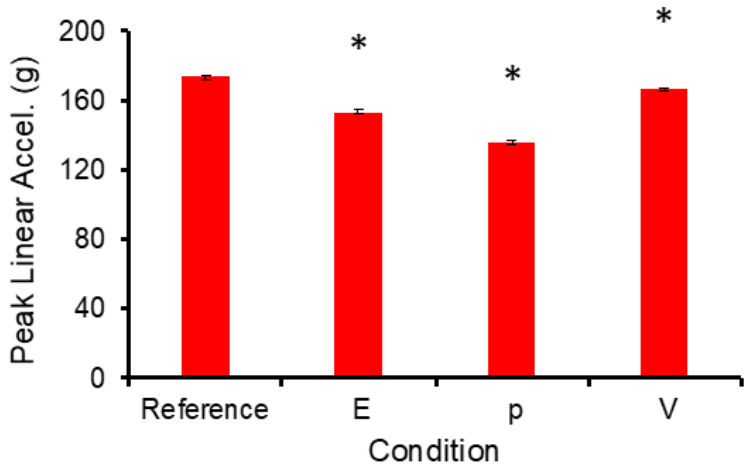

Fig. 6 Mean ± 1 standard deviation (SD) of peak linear acceleration of the DOT-C headform dropped onto a MEP pad. Conditions are those presented in Table 1. The * represents a statistical difference from the reference condition; alpha level ≤ 0.05.

4.2 Accounting for Drop Mass: Different ATD Geometry

Statistical analysis revealed that there was unlikely a meaningful interaction between drop mass and location for cases in which the drop energy was matched between the monorail and basket drop impacts ($p = 0.146$, Greenhouse–Geisser; $\eta_p = 0.28$). However, a main effect of drop mass was observed to be relatively large ($p < 0.001$; $\eta_p = 0.99$). On average, the difference in PLA between the basket drop and monorail was 94.2 (86.8–101.6) g (Fig. 7).

We observed an interaction between drop mass and location for cases in which the drop velocity was matched between the basket drop and monorail was ($p = 0.019$, Greenhouse–Geisser; $\eta_p = 0.48$). Additionally, we observed a main effect of mass (i.e., monorail vs. basket drop [$p = 0.012$; $\eta_p = 0.68$]). However, on average the difference in PLA between the monorail and basket drop was 7.8 (2.4–13.3) g. Simple effects indicated that the monorail and basket drop methods statistically

differed at the crown, rear, left nape, and right nape locations, but not at the front, left-side, and right-side locations (Fig. 7).

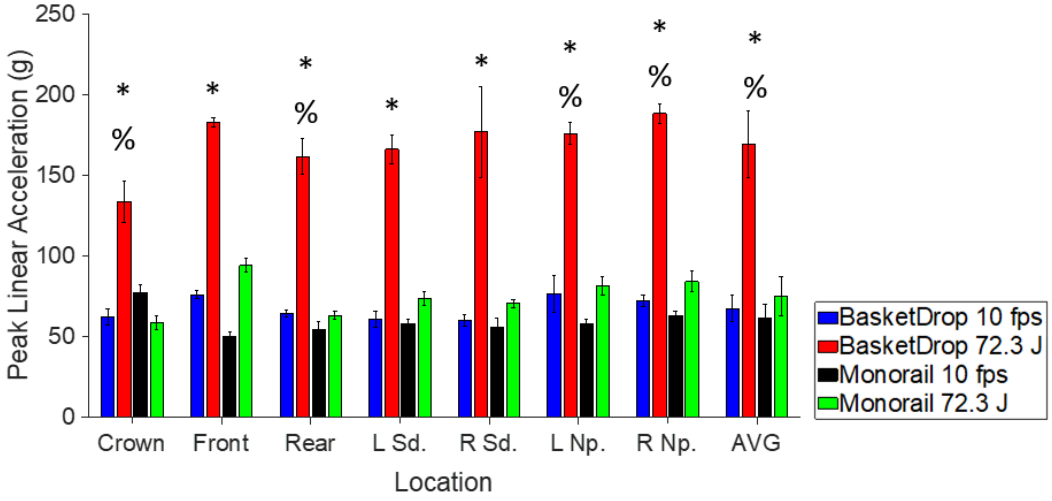

Fig. 7 Mean ± 1SD of peak linear acceleration for the *basket* and *monorail with neck* drop impact tests of a male 50% Hybrid III head donning an ACH. The * indicates a statistical difference between energy matched basket drop and monorail. % indicates a statistical difference between velocity matched basket drop and monorail. Differences at the average indicate a main effect.

4.3 Velocity Matched Results across Methods

The interaction between impact location and machine configuration was significant for PLA ($p < 0.001$, $\eta^2 = 0.48$), PAA ($p < 0.001$, $\eta^2 = 0.41$), and PAV ($p < 0.001$, $\eta^2 = 0.90$). Furthermore, the main effect of machine configuration was significant for PLA ($p < 0.001$, $\eta^2 = 0.87$), PAA ($p < 0.001$, $\eta^2 = 0.76$), and PAV ($p < 0.001$, $\eta^2 = 0.91$). Pairwise comparisons revealed that the pneumatic ram typically had lower PLA and PAA values than the basket drop or guided monorail (Figs. 8 and 9). In contrast, the basket drop typically (four out of seven locations) had lower PAV values (Figs. 10 and 11). Such differences seem to occur because impacts on the basket drop resulted in less rotation of the head than on the pneumatic ram or monorail. For the rotational measures (PAA and PAV), the monorail configuration typically had the greatest values. Note figure values represent the estimated mean for each measure after accounting for the variance due to velocity. See the supplementary material (Figs. A-13 to A-18 in the Appendix) for the plots of each measure across configurations at each location at each impact velocity. Figure 11 shows the resultant angular velocity rear impact curves.

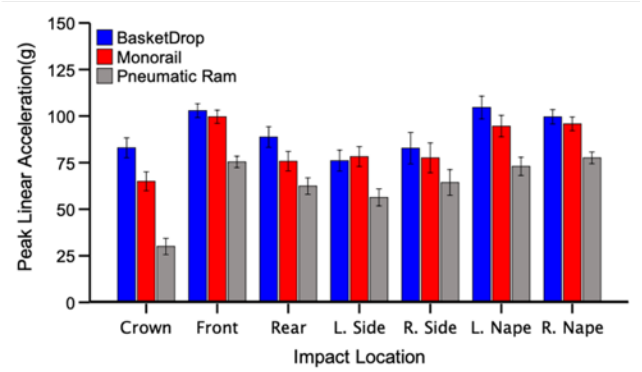

Fig. 8 Estimated mean of PLA ± 95% CI

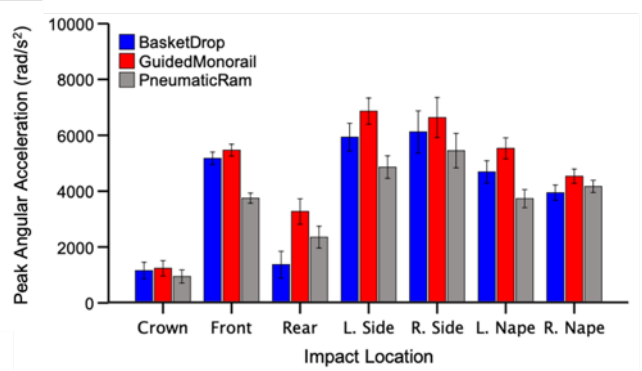

Fig. 9 Estimated mean of PAA ± 95% CI

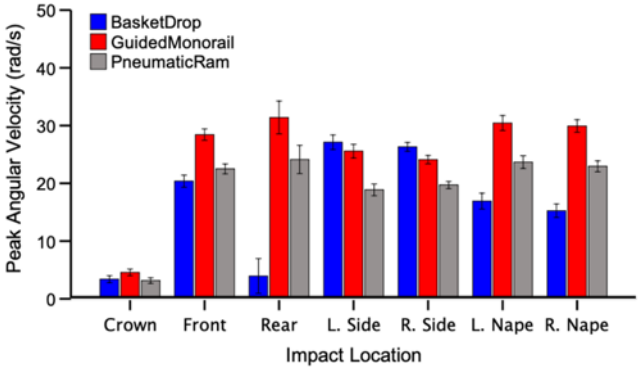

Fig. 10 Estimated mean of PAV ± 95% CI

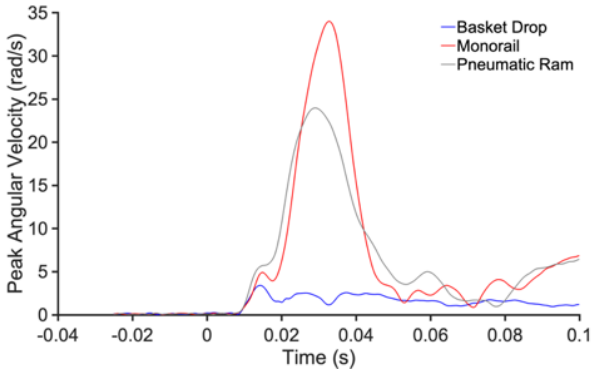

Fig. 11 Resultant angular velocity rear impact curves

5. Discussion

5.1 Accounting for Drop Mass

Despite differences in drop mass, matching impact velocity across drop tests of the same ATD resulted in PLA values that were most similar compared to matching the impact energy or momentum of the drop. When an ATD head (male 50% Hybrid III) of two different geometries (with and without a neck), masses, and boundary conditions (neck attached to head and guided rail and head resting on basket ring) were dropped onto a semi-rigid anvil, matching the kinetic energy between the two ATD complexes resulted in dramatically different PLA responses at all impact locations. However, when the drops were matched by velocity, the mean difference in PLA was markedly less and no statistical differences were found at three of the seven impact locations.

These results are somewhat in line with the predictions of Eq. 1, which indicate that drop mass does not influence PLA values. However, we did find that in both the identical ATD scenarios (DOT-C) and an ATD (male 50% Hybrid III) that was modified to have different geometries and boundary conditions, velocity matching still resulted in PLA values that differed according to a critical alpha value of 0.05. Such differences may be explained by interactions between the mass and the boundary conditions as well as characteristic responses of the impacted materials, which are not accounted for in Eq. 1. Nevertheless, it seems that matching the velocity across drop impacts results in a much closer match between PLA values across ATD complexes and drop methods relative to matching momentum or energy. The relatively similar PLA values across drop masses when velocity is matched allows for a more realistic or authentic comparison between different drop methods and ATDs in regard to other output measures such as PAA and PAV.

5.2 Equations Governing Velocity Matched Impacts across Methods

The pneumatic ram and drop responses are influenced by multiple factors and boundary conditions. A simplified model of the response will be helpful to understand the results of the velocity matched data across methods. We can simplify the linear and angular acceleration–time curve response by expressing the response as a half-sine wave.[22] The general expression of the acceleration pulse of such a body is as follows[22]:

$$A(t) = PAsin\frac{\pi}{\tau}t \tag{2}$$

where A(t) is the acceleration time curve, PA is the peak acceleration, and τ is the duration of the acceleration–time curve. Equation 2 can be solved for the change in velocity as follows[2]:

$$\Delta V = \frac{2PA\tau}{\pi} \tag{3}$$

where ΔV is the difference between the body's initial and final velocity. Note the equations presented in the following discussion are all based on Eq. 3.

5.2.1 Equations Governing Velocity Matched Drop Impacts

When an ATD is dropped onto an anvil (anchored to ground), it makes contact at a prescribed velocity, then slows, comes to a stop, and rebounds. Furthermore, the ATD will rotate after impact if the impact force does not pass through the ATD center of gravity or pivot joints.

In such a case, the PLA of an ATD that rebounds is shown in Eq. 4, while Eq. 5 shows the PLA for an ATD that does not rebound:

$$\mathrm{PLA_{Rebound}} = \frac{\Delta \mathrm{V}\pi}{2\tau} \tag{4}$$

$$\mathrm{PLA_{No-rebound}} = \frac{\mathrm{V}_i\pi}{2\tau} \tag{5}$$

where ΔV is the difference between the ATD impact velocity (V_i) and peak rebound velocity (V_f). Note the sign of the rebound velocity and initial velocity will differ. Equation 4 is just a reordering of the terms of Eq. 3. Equations 4 and 5 indicate that with all other factors constant, an impact that results in greater rebound velocity will also have greater PLA. Thus, helmet and anvil materials that help to transfer impact energy away from the head will work to reduce ΔV and consequentially PLA.

Regardless of rebound, the conservation of angular momentum equation can be leveraged to express Eq. 3 in a form for the PAA of an ATD dropped onto an anvil as follows:

$$\text{PAA} = \frac{m_{ATD} V_i \text{R}\pi}{2\tau I_{ATD}} \tag{6}$$

where m_{ATD} is the mass of the ATD, R is the perpendicular distance between the impact vector and the axis of rotation, and I_{ATD} is the ATD's moment of inertia, where I_{ATD} is the product of the total mass of the ATD complex and the square of the effective radius of gyration. Equation 6 indicates that PAA will increase as impact velocity and the distance between the impact vector and the axis of rotation increase. Notably, Eq. 6 indicates that changes in the helmet mass or geometry will likely have an influence on PAA if the ratio between m_{ATD} and I_{ATD} does not remain constant.

5.2.2 Equations Governing Velocity Matched Pneumatic Ram Impacts

In cases where the ATD is at rest and impacted by a moving impactor, as with the pneumatic ram, Eq. 3 and the conservation of momentum equations can be used to calculate the PLA and PAA when the acceleration response is simplified to a half-sine wave as follows:

$$\text{PLA} = \frac{m_r (\Delta \text{V}_{IR})\pi}{2\tau m_{ATD}} \tag{7}$$

$$\text{PAA} = \frac{m_r (\Delta \text{V}_{IR})\text{R}\pi}{2\tau I_{ATD}} \tag{8}$$

where m_r is the mass of the impactor ram; m_{ATD} is the mass of the ATD including its mount, sliding table, and helmet (ATD-complex); and ΔV_{IR} is the difference between the impactor ram's impact velocity and its velocity at the end of the impact. Equations. 7 and 8 indicate that the ratio of m_r to m_{ATD} for a typical ATD must be greater than 1 for PLA and PAA values on the pneumatic ram to be comparable to those from drop impacts.

5.3 Velocity Matched Results across Methods

Generally, we found that the peak headform linear and angular accelerations were less for the pneumatic ram impacts compared to the drop impacts, but that peak angular velocity was typically less for the basket drop method. As indicated by the previous equations, it is likely that the differences in boundary conditions resulted in lower PLA and PAA for the pneumatic ram.

In our drop tests, the ATD rebounded as indicated by a sign change in linear velocity of the center of mass of the headform. In our ram impacts, the ATD started

at rest and then accelerated away from the impactor. Data from the primary axis of movement from a subset of impacts at 14 ft/s showed a moderate to strong association between ΔV and PLA, which highlights the link between the change in ATD velocity and PLA (Eq. 3 and Fig. 12).

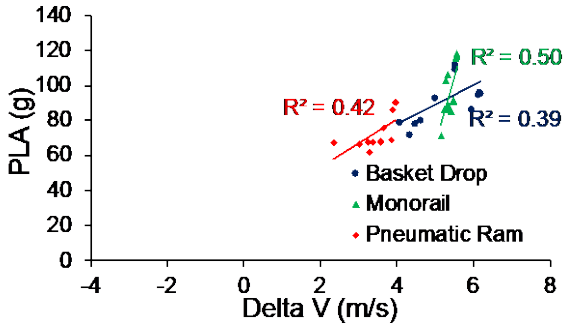

Fig. 12 Association between ΔV of the ATD and PLA for a subset of drop impacts at 14 ft/s with the basket drop, monorail, and pneumatic ram methods

Averaged across impact locations, PAA was greater for the monorail than basket drop method. Qualitative analysis of high-speed video indicated that for the monorail impacts, in which the neck was attached to the tower, the axes of rotation included the cervical vertebrae, atlanto-occipital joints, and head center of mass. In contrast, the ATD rotated only about the headform's center of mass in the basket drop method. Based on these observations, the R value (see Eq. 6) was greater for the monorail impacts than for the basket drop impacts (Fig. 13). Consequentially, this difference likely contributed to the greater PAA for the monorail method. However, the differences in PAA between the monorail and basket drop methods may have been limited by the greater moment of inertia length variables of an ATD with than without a neck (Eq. 6).

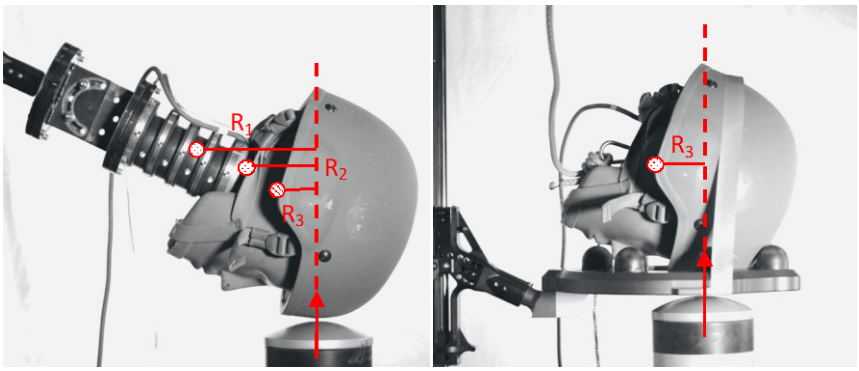

Fig. 13 Perpendicular distance, R from impact vector to points of rotation for the monorail (left) and basket drop (right) methods

In the pneumatic ram tests, the ratio of impactor mass to ATD-complex mass was 0.96. Thus, as predicted from the Eqs. 7 and 8 the pneumatic ram test resulted in the lowest PLA and PAA values.

Post hoc analysis with FEA modeling served to validate our finding and also provide limits on the extent Eqs. 3–8 could help to explain our findings. Increasing the mass of a simulated impactor by four times, from 16.7 kg to 66.8 kg, and impacting an ATD-complex of mass 23.6 kg increased PLA by 15.8%, PAA by 13.4%, and PAV by 30.2%, as is expected from Eqs. 7 and 8. Additionally, FEA simulations of the front and left side impacts at 14 ft/s, which matched impactor mass to ATD-complex mass for the pneumatic ram impacts did not consistently match those values obtained in the experimental drop tests. Such a finding seems to contradict the previous equations in that Eq. 7 (PLA for pneumatic ram) simplifies to Eqs. 4 and 5 (PLA for drop methods) when ATD mass is equivalent to impactor mass for the pneumatic ram. The findings also indicate that the additional parameters likely influence the results and highlight the limits of these equations in predicting PLA and PAA values. Similarly, we did not find a match between FEA model PAA for the pneumatic ram and experimental drop PAA values when ATD-complex mass was matched to impactor mass. However, the inertial properties of the ATD complex in the drop methods do not match the inertial properties of the impactor in the pneumatic ram method as would likely be needed to obtain similar results between the two methods (see Eqs. 6 and 8). Overall, these findings highlight the influence that ATD and impactor mass and inertial properties have on peak resultant kinematics.

The pneumatic ram impacts likely resulted in overall lower accelerations values than the drop impact methods partly because of the ram's lower mass relative to the ATD-complex in that format. While ATD mass has the potential to have little influence on the linear kinematics of drop impacts, the addition of inertial components to the ATD seem to alter its angular kinematic response. Specifically, the neck component likely works to increase the perpendicular distance between the impact vector and the axis of rotation, thus increasing PAA for the monorail compared to basket drop method. Importantly, these mechanisms will likely result in similar results across sensor platforms if proper consideration is given to the filtering scheme between the different sensor platforms.

6. Conclusion

In order to characterize and ultimately determine the efficacy of combat helmets to mitigate brain injury from blunt impacts, kinematic measures of head rotation should be quantified during the impact event. We have detailed three methods using

commercially available drop and collision machines, which can replicate the Army ATD head positions and impact locations used to currently test linear head acceleration during blunt impacts. In doing so, we have also described a universal method by which to describe the ATD pose for blunt impact tests. Our results indicate that a like-for-like comparison across methods, especially drop methods, is achieved by matching the velocity of impact. Additionally, we observed that the pneumatic ram method typically resulted in linear and angular kinematics that are less than the drop methods, though this was largely due to the ratio of impactor to ATD mass. The monorail method typically resulted in the greatest angular kinematics. Such results are in line with the equations of motion but observed deviations for the general trends are likely a result of differences in boundary conditions that were not accounted for in the presented equations of motion.

7. References

1. US Army Program Executive Office-Soldier SE. Advanced Combat Helmet (ACH) purchase description. US Army Program Executive Office-Soldier SE; 2010. Report no.: AR/PD 10-02.
2. Bruggeman M. ATC-MMTB-029. Blunt impact testing procedure for combat helmets. Internal Operating Procedure No.: 029 REV E. Aberdeen Test Center; 2013. p 1–25.
3. Viano DC, Casson IR, Pellman EJ, Zhang L, King AI, Yang KH. Concussion in professional football: brain responses by finite element analysis: part 9. Neurosurgery. 2005;57(5):891–915.
4. Hardy WN, Mason MJ, Foster CD, Shah CS, Kopacz JM, Yang KH, King AI. A study of the response of the human cadaver head to impact. Stapp Car Crash J. 2007;51:17–80.
5. Holbourn AHS. Mechanics of head injuries. Lancet. 1943;242(6267):438–441.
6. Takhounts EG, Ridella SA, Hasija V, Tannous RE, Campbell JQ, Malone D, Danelson K, Stitzel J, Rowson S, Duna S. Investigation of traumatic brain injuries using the next generation of Simulated Injury Monitor (SIMon) finite element head model. Stapp Car Crash J. 2008;52:1–31.
7. Marine Corps Systems Command, Product Manager, Infantry Combat Equipment. Enhanced Combat Helmet (ECH) purchase description. Marine Corps (US); 2016. Report No.: GL-PD-09-04M.
8. Lurski AJ, Plaisted TA, Wetzel ED. Combat helmet padding systems response under multiple blunt-impact events. CCDC Army Research Laboratory; 2020. Report No: ARL-TR-8998.
9. NOCSAE. Standard pneumatic ram test method and equipment used in evaluating the performance characteristics of protective headgear and face guards NOCSAE; 2019. Report No.: ND 081-18am19a. https://nocsae.org/wp-content/uploads/2018/05/ND081-18am19a-Standard-Pneumatic-Ram-Test-Method-003.pdf.
10. Bland ML, McNally C, Zuby DS, Mueller BC, Rowson S. Development of the STAR evaluation system for assessing bicycle helmet protective performance. Ann Biomed Eng. 2020;48(1):47–57. doi:10.1007/s10439-019-02330-0.

11. Adanty K, Clark JM, Post A, Hoshizaki TB, Gilchrist MD. Comparing two proposed protocols to test the oblique response of cycling helmets to fall impacts. Int J Crashworthiness. 2019;0(0):1–16.

12. The test lab. Mips; n.d. [accessed 2021 June 7]. https://mipsprotection.com/science-technology/test-lab.

13. Hoge CW, McGurk D, Thomas JL, Cox AL, Engel CC, Castro CA. Mild traumatic brain injury in U.S. soldiers returning from Iraq. N Engl J Med. 2008;358(5):453–463.

14. Ivins BJ, Schwab KA, Warden D, et al. Traumatic brain injury in U.S. Army paratroopers; prevalence and character. J Trauma. 2003;55(4):617–621.

15. TBICoE. DoD numbers for traumatic brain injury, worldwide - totals; 2000-2020 Q1-Q4. Traumatic Brain Injury Center of Excellence; 2021 Aug 26.

16. NOCSAE. Standard test method and equipment used in evaluating the performance characteristics of headgear/equipment. NOCSAE; 2017. Report No.: ND 001-17m17b. https://nocsae.org/wp-content/uploads/2018/05/1514996961ND00117m17bDropTestMethod.pdf.

17. Bliven E, Bourdet N, Deck C, Madey SM. A novel strategy for mitigation of oblique impacts in bicycle helmets forensic biomechanics. Artic J Forensic Biomech. 2019;10:1.

18. Halldin P, Kleiven SS. The development of next generation test standards for helmets. In: Proceedings of the 1st International Conference on Helmet Performance and Design; 2013 Feb 15; London, UK. http://www.diva-portal.se/smash/get/diva2:1276564/FULLTEXT01.pdf.

19. Denavit J, Hartenberg RS. A kinematic notation for lower-pair mechanisms based on matrices. ASME Journal of Applied Mechanics. 1955;77:215–221.

20. Spong MW, Hutchinson S, Vidyasagar M. Robot modeling and control. Wiley; 2006.

21. Jesunathadas M, Gould TE, Plaisted TA, Edwards ED, Piland SG. Describing headform pose and impact location for blunt impact testing. J Biomech. 2020;109:109923.

22. Lalanne C. Mechanical shock. 3rd ed. John Wiley & Sons, Ltd; 2014 (vol. 2).

Appendix. Supplementary Material

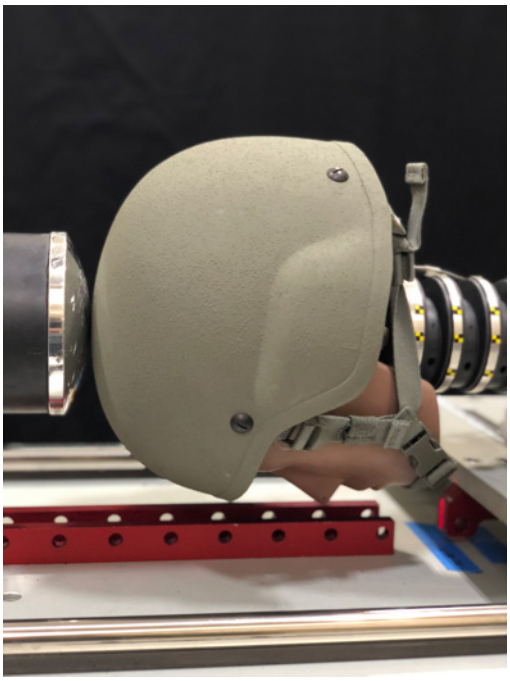

Fig. A-1 Pneumatic ram machine configuration with male 50% Hybrid III head and neck anthropomorphic test device (ATD) in pose for the crown impact location

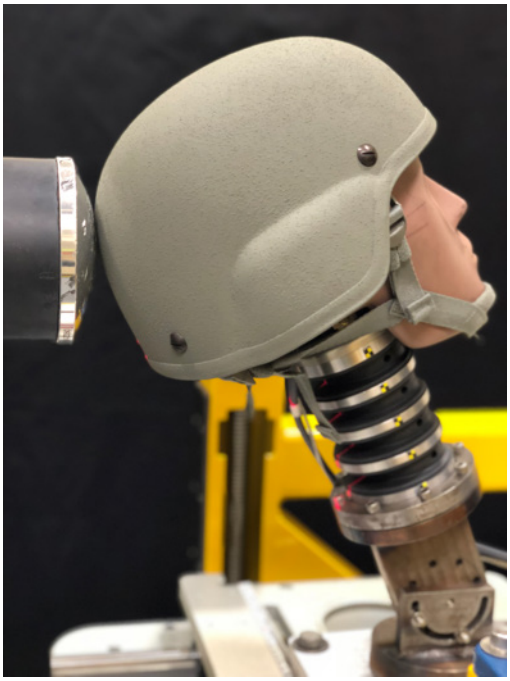

Fig. A-2 Pneumatic ram machine configuration with male 50% Hybrid III head and neck ATD in pose for the rear impact location

Fig. A-3 Pneumatic ram machine configuration with male 50% Hybrid III head and neck ATD in pose for a side impact location

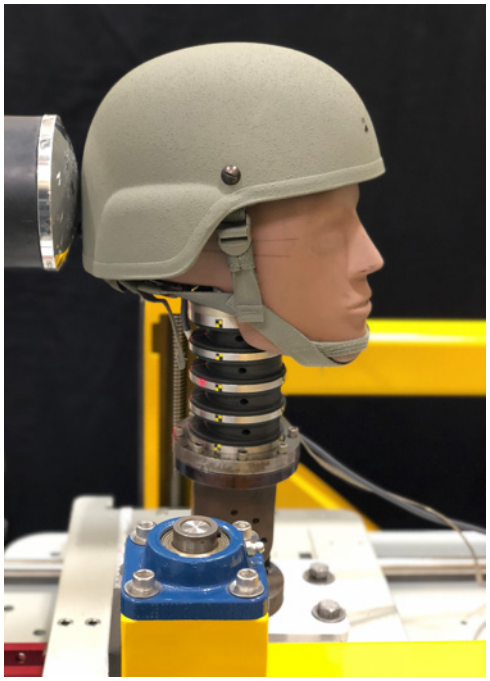

Fig. A-4 Pneumatic ram machine configuration with male 50% Hybrid III head and neck ATD in pose for a nape impact location

Fig. A-5 Monorail with neck configuration with male 50% Hybrid III head and neck ATD in pose for the crown impact location

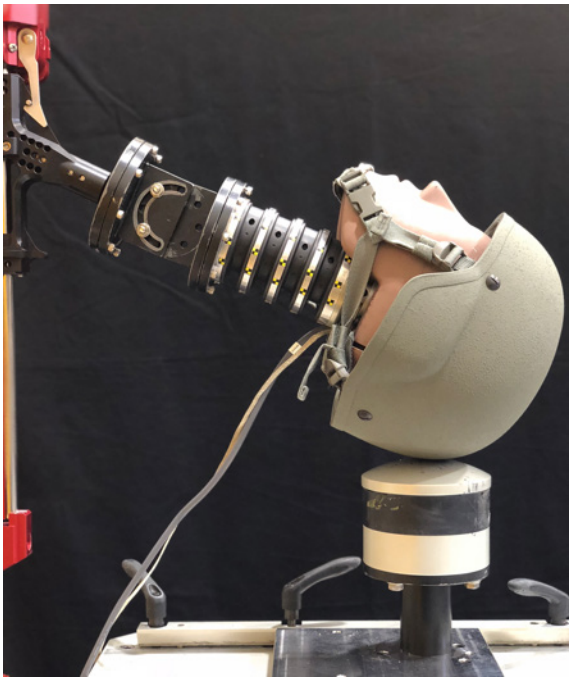

Fig. A-6 Monorail with neck configuration with male 50% Hybrid III head and neck ATD in pose for the rear impact location

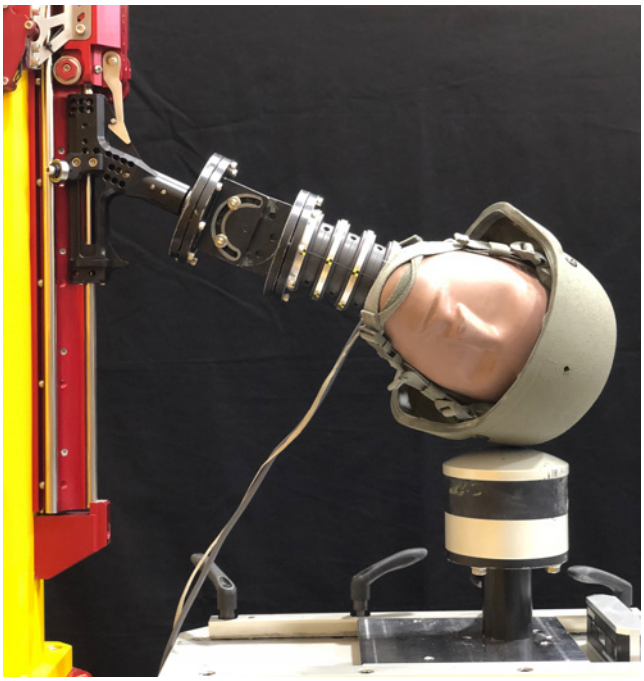

Fig. A-7 Monorail with neck configuration with male 50% Hybrid III head and neck ATD in pose for a side impact location

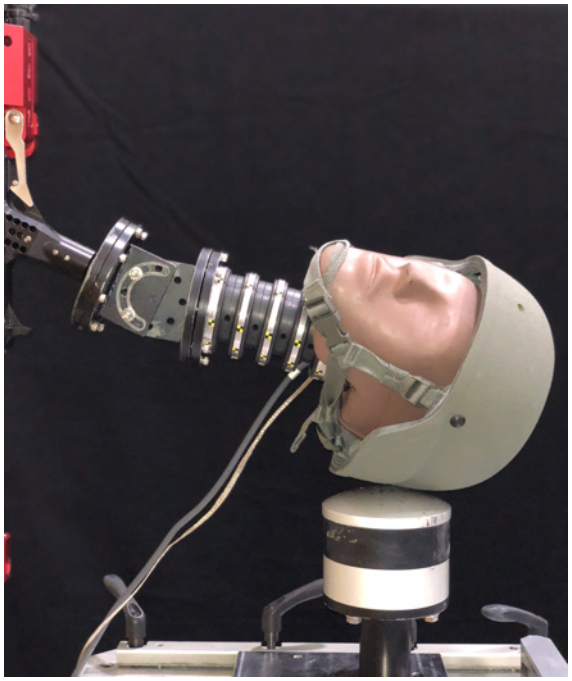

Fig. A-8 Monorail with neck configuration with male 50% Hybrid III head and neck ATD in pose for a nape impact location

Fig. A-9 Basket drop configuration with male 50% Hybrid III head and neck ATD in pose for the crown impact location

Fig. A-10 Basket drop configuration with male 50% Hybrid III head and neck ATD in pose for the rear impact location

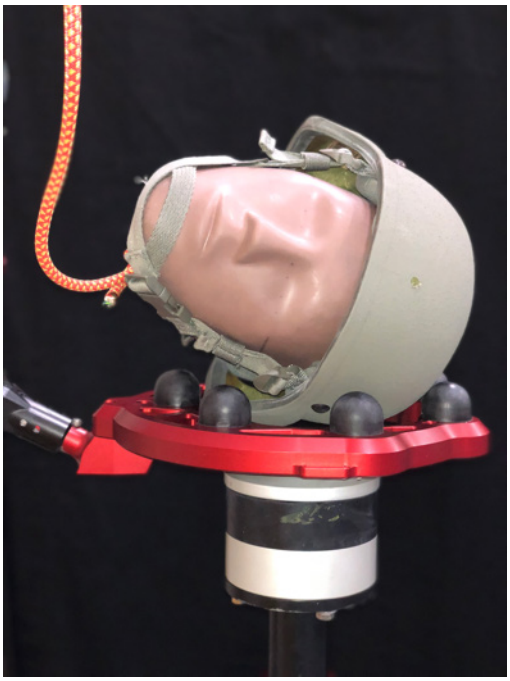

Fig. A-11 Basket drop configuration with male 50% Hybrid III head and neck ATD in pose for a side impact location

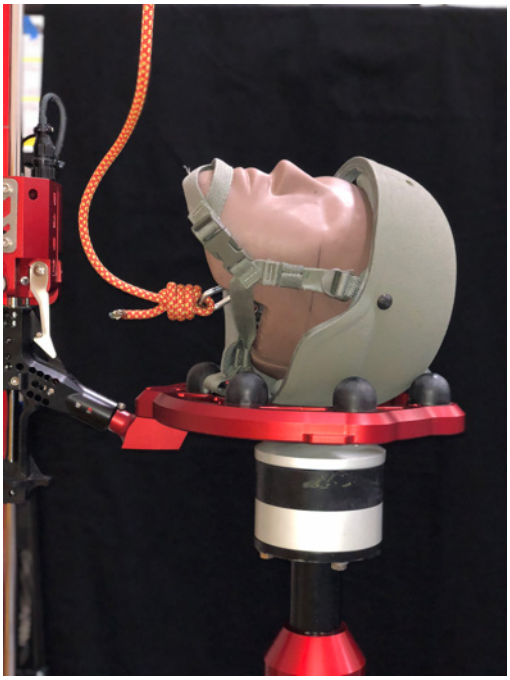

Fig. A-12 Basket drop configuration with male 50% Hybrid III head and neck ATD in pose for a nape impact location

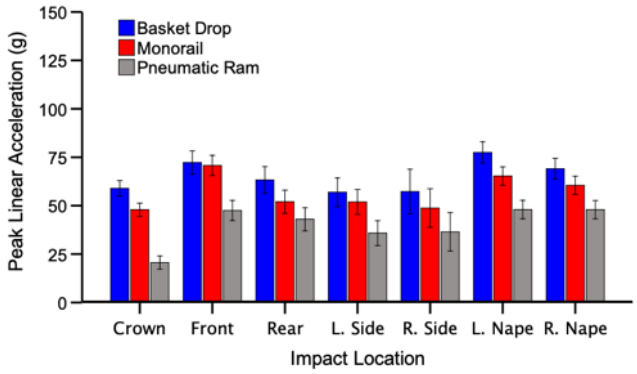

Fig. A-13 Estimated mean of PLA ± 95% confidence interval (CI) at 10 ft/s

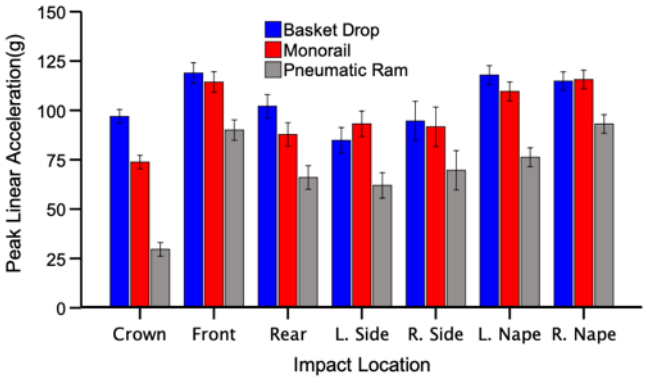

Fig. A-14 Estimated mean of (PLA) ± 95% CI at 14 ft/s

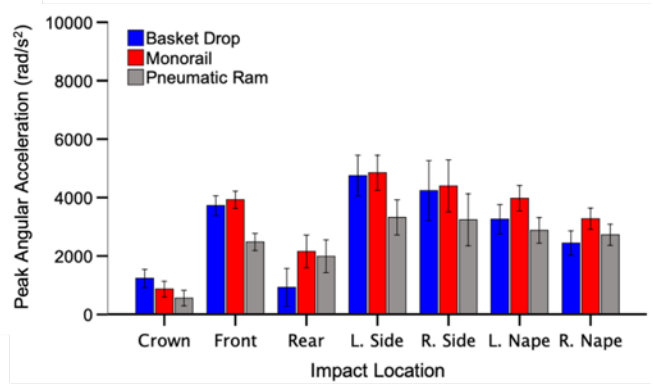

Fig. A-15 Estimated mean of peak angular acceleration (PAA) ± 95% CI at 10 ft/s

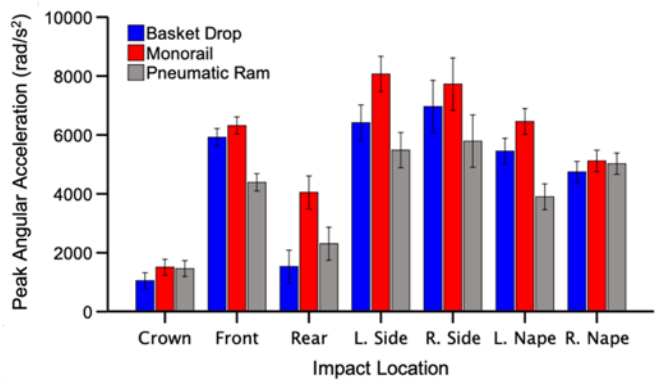

Fig. A-16 Estimated mean of PAA ± 95% CI at 14 ft/s

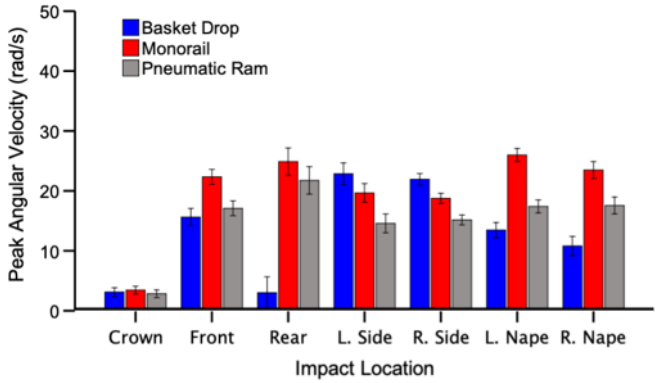

Fig. A-17 Estimated mean of peak angular velocity (PAV) ± 95% CI at 10 ft/s

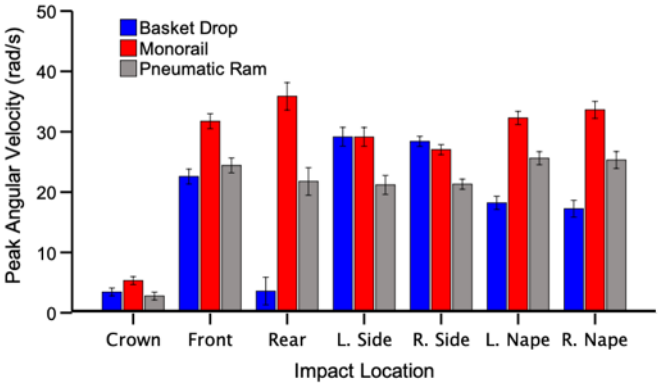

Fig. A-18 Estimated mean of PAV ± 95% CI at 14 ft/s

List of Symbols, Abbreviations, and Acronyms

6DOF	6 degree of freedom
ACH	Advanced Combat Helmet
ANCOVA	analysis of covariance
ANOVA	analysis of variance
ARL	Army Research Laboratory
ATD	anthropomorphic test device
CI	confidence interval
CORA	Correlation and Analysis Software
DEVCOM	US Army Combat Capabilities Development Command
DH	Denavit–Hartenberg
DOT	Department of Transportation
FE	finite element
FEA	finite element analysis
MEP	Modular Elastic Programmer
NFL	National Football League
NOCSAE	National Operating Committee on Standards and Equipment
PAA	peak resultant angular accelerations
PAV	peak resultant angular velocity
PLA	peak resultant linear acceleration
SD	standard deviation
TBI	traumatic brain injury

1 (PDF) DEFENSE TECHNICAL INFORMATION CTR
DTIC OCA

1 (PDF) DEVCOM ARL
FCDD RLD DCI
TECH LIB

14 (PDF) DEVCOM ARL
FCDD RLW MA
R NEICE
TA BOGETTI
SE BOYD
TA PLAISTED
JM STANISZEWSKI
M YEAGER
E WETZEL
A LURSKI
FCDD RLW TB
M KLEINBERGER
S SATAPATHY
T ZHANG
D KRAYTERMAN
K RAFAELS
FCDD RLW B
C HOPPEL
FCDD RLW PE
P GILLICH
FCDD RLW MB
D O'BRIEN

4 (PDF) PROG EXECUTIVE SOLDIER OFC
J HOPPING
T SMITH
A DE GROOT
B SUNDERBERG

10 (PDF) DEVCOM NATICK SOLDIER SYSTEMS CTR
D COLANTO
R DILALLA
J KIREJCZYK
J PARKER
M MAFFEO
B FASEL
C HEWITT
M ROTH
S BENNET
D OTTERSON